

## Idealized Plasma Problems for Magnetohydrodynamic Code Verification

Pavlos G. Mikellides, Department of Mechanical and Aerospace Engineering, Arizona State University,  
[Pavlos.Mikellides@asu.edu](mailto:Pavlos.Mikellides@asu.edu)

### Abstract

The closed-form analytic solutions to two idealized plasma problems are presented as test cases for verification and benchmarking of magnetohydrodynamic computer codes. The first problem addresses magnetic diffusion with joule heating designed to produce a diverging temperature profile so as to significantly challenge the stability and accuracy limitations of different numerical schemes. The second problem is the classic magneto-shock tube problem for which an explicit analytic solution is derived. This allows a simple and unique presentation of the solution that can be easily utilized. A magnetohydrodynamic code is employed to model the problems and comparisons of the numerical results serve as bi-lateral validation of the analytic and numerical solutions. Furthermore, these comparisons serve as a reference standard for accuracy and overall code performance.

### Nomenclature

A = propagation speed  
B = magnetic induction  
L = computational length  
P = full pressure  
R = specific gas constant  
T = temperature  
 $V_A$  = Alfvén speed  
 $V_s$  = Shock speed  
a = speed of sound  
e = specific internal energy  
p = thermal pressure  
u = flow velocity  
t = time

$\gamma$  = ratio of specific heats  
 $\Delta z, \Delta i$  = grid cell dimensions  
 $\eta$  = electrical resistivity  
 $\bar{\eta}$  = magnetic diffusivity  
 $\nu$  = Courant number  
 $\mu_0 = 4\pi \times 10^{-7}$  H/m  
 $\rho$  = mass density  
 $\zeta$  = degree of ionization  
i,j,k = arbitrary coordinates  
x,y,z = Cartesian coordinates  
r,  $\theta$ , z, = cylindrical coordinates

### Introduction

One of the essential procedures in the development and assessment of computational fluid dynamic (CFD) or magnetohydrodynamic (MHD) codes is verification and benchmarking. This is accomplished by comparisons to idealized problems for which exact analytic solutions are accessible and subsequent performance evaluation in terms of both accuracy and computational resource requirements. The limitation of such idealized problems is that they can address only particular physical processes as opposed to the global coupled solution that such codes aim to produce. Thus, adequate assessment of such numerical tools should incorporate the maximum possible number of appropriately chosen problems. Consequently, the usefulness of such test problems relies in the simplicity of implementation, range in applicability to several code components and their ability to extend testing a code's capabilities towards possible limitations.

The two essential physical processes in MHD flows are magnetic diffusion and convection. Their coupling ultimately determines the overall behavior of most physical problems ranging from space physics to MHD power generation and acceleration. It is thus critical that MHD codes accurately capture such processes which when fully expanded involve time-dependent interactions of a three dimensional magneto-fluid subject a tensor magnetic diffusivity. The objective of this paper is to present the solution to two idealized problems that can serve in verifying the accuracy and performance of these processes. The design and presentation aims to maximize simplicity without loss of value in testing the relevant numerical schemes.

The first test case addresses time-dependent magnetic diffusion from a constant field boundary combined with joule heating. The solution is very simple but the inclusion of joule heating without other dissipative effects produces a diverging temperature profile that can serve in stressing the capabilities of a MHD code. Moreover, it can be equally used for all directions within both planar and cylindrical geometries. The second problem is the classic shock tube problem<sup>1</sup> that has long been identified as an ideal problem in testing the solution to hyperbolic partial differential equations. It has been extensively utilized to test both hydrodynamic<sup>2</sup> and magnetohydrodynamic<sup>3</sup> numerical schemes as it allows assessment of capturing different types of discontinuities. However, the literature lacks of the solution to this problem in terms of a specific closed-form analytic expression that can be directly applied. The reason is probably two-fold; a) the solution involves derivative discontinuities, and b) the solution is implicit. Consequently, the solution to the problem is usually presented in general terms where an iterative procedure is implied, the results are presented but the specific algorithm is absent. The complexity is compounded for magneto-fluids where no analytic solution has yet been established for any gas. However, for the special case of a  $\gamma=2$  gas the solution is accessible and can be used to verify MHD codes. So, the approach outlined herein produces a closed-form analytic solution to the shock tube problem that can be easily implemented. Further, an explicit solution is achieved without loss of generality and value for the test case and it can still be utilized to benchmark both CFD and MHD computer codes.

The utility and validity of these idealized problems is addressed by comparisons to a sophisticated MHD code with significant pedigree in a wide variety of plasma problems. Such comparisons can also serve as a reference to expected performance from other codes. So, the paper first presents a pertinent description of the MACH code followed by the detailed description and application of the two test problems.

## Numerical Model

The Multi-block Arbitrary Coordinate Hydromagnetic (MACH) code<sup>4</sup> is a time-dependent, multi-material, non-ideal MHD solver that can address complex geometric configurations.<sup>5</sup> The more mature two-dimensional axisymmetric version has recently been upgraded to a full three-dimensional code. A wide range of geometries is managed by partitioning the physical region in block-like sub-domains which are mapped to logical rectangular blocks that constitute the computational region. The computational grid can be adaptive to dynamically resolve regions of varying characteristic scales and can move in an Arbitrary-Lagrangian-Eulerian (ALE) fashion based on a user-defined grid speed relative to the flow speed.

The code incorporates a variety of sophisticated physics which are briefly outlined as they are not particularly pertinent to the idealized benchmark cases described herein. The mass continuity and momentum equations assume a compressible, viscous fluid with the latter including both real and artificial viscosity effects. The stress tensor can be chosen to evolve under elastic stress for strength of material calculations<sup>6</sup> or modeled as a viscous stress tensor for Newtonian fluid to upgrade the code to a Navier-Stokes solver.<sup>7</sup> The electrons, ions and radiation field are in thermal non-equilibrium, so MACH solves up to three energy equations. These include thermal conduction with anisotropic transport and three different models for radiation cooling; optically-thin Planck radiation, equilibrium and non-equilibrium diffusion radiation.<sup>8</sup> Evolution of the magnetic field is prescribed by the induction equation that includes resistive diffusion, the Hall effect and the thermal source for magnetic fields. Various models for the plasma resistivity are available. They comprise classical anisotropic resistivity,<sup>9</sup> several anomalous resistivity models and contributions from electron-neutral collisions applicable to weakly ionized gases.<sup>10</sup> In many engineering applications the source of magnetic flux is applied currents produced from externally-applied voltage differentials. For this, the code includes a variety of circuit models such as LRC, Pulse-Forming-Networks, sine-waveforms and several others. The set of the MHD equations is completed by functional relationships for the equations of state that can be either analytic or tabular. The SESAME library<sup>11</sup> is the tabular model that includes semi-empirical models for the thermodynamic properties, transport coefficients, (including opacities) and average ionization state under local thermodynamic equilibrium.

The numerical techniques<sup>2</sup> invoke a fractional time-stepping algorithm for time advance and differencing while the spatial differencing of the equations is carried out by the finite control volume approach. The time advance technique allows mixed explicit-implicit, so diffusive processes along with the hydrodynamics are implicitly differenced to alleviate highly restrictive constraints. On the other hand, less numerically restrictive processes such as convective transport are explicitly differenced. Specifically, magnetic diffusion is time-differenced as follows:

$$\bar{B}(t + \delta t) = \bar{B}(t) - \Delta t \left[ \beta \bar{\nabla} \times \left( \bar{\eta}(t) \cdot \bar{\nabla} \times \bar{B}(t + \delta t) \right) + (1 - \beta) \bar{\nabla} \times \left( \bar{\eta}(t) \cdot \bar{\nabla} \times \bar{B}(t) \right) \right] \quad (1)$$

where  $\delta t < \Delta t$  is the fractional time step and  $0 \leq \beta \leq 1$  determines the degree of explicit/implicit mixing. The value for  $\beta$  is determined by the factor  $\phi = \frac{\bar{\eta} \Delta t}{\Delta j^2}$  where  $\Delta j$  is the smallest dimension of the grid's cell at which each

computation takes place. For  $\phi < 3/4$  the differencing is explicit, for  $\phi > 5/4$  the differencing is implicit, while for other values the algorithm is mixed explicit-implicit. Spatially, the scheme is central differenced so the truncation error is  $\mathcal{O}[\Delta t, \Delta j^2]$  where  $j$  is any of the three dimensions. The solution is obtained by a block Jacobi Successive Over-Relaxation (SOR) iteration.<sup>12</sup> The convergence is accelerated by implementation of the Full Approximation Storage (FAS) multi-grid algorithm.<sup>13</sup> The multi-grid algorithm performs iterations by consecutively reducing the grid's dimensions by half, thus producing different levels of coarser grid. At each level the Jacobi iteration produces larger corrections. The inviscid hydrodynamics,

$$\rho \frac{\partial \vec{u}}{\partial t} = -\vec{\nabla}(\rho + \mu_A) + \frac{1}{\mu_0} (\vec{\nabla} \times \vec{B} \times \vec{B}) \quad (2)$$

where  $\mu_A$  represents the artificial viscosity term, utilize the same implicit method to time-fractionally advance the velocity field. Unlike the diffusive processes however, the scheme is fully-implicit and utilizes central time differencing to produce truncation error  $\mathcal{O}[\Delta t^2, \Delta j^2]$ . The convective transport of mass, momentum, energy and magnetic fluxes can be computed via two different numerical schemes; a simple first-order donor-cell method or a second-order Van Leer<sup>14</sup> scheme. The choice should be evaluated for each case based on the relative magnitude of dissipation associated with the first-order scheme or dispersive oscillations associated with the second-order scheme.

Boundary conditions are implemented by the ghost-cell technique which circumvents the need for special treatment due to the different physical laws applicable at the boundaries. The computational grid is extended by one additional row, the ghost row, in all three directions. The physical processes that govern an individual boundary can then be directly imposed in these additional ghost cells via simple expressions. The technique obviously requires a slightly elevated storage capability along with some elevated computational times but they are greatly overshadowed by the advantages. Besides the simplicity associated with the application and modification of boundary conditions, the ghost-cell technique is the essential tool in allowing computations in discrete blocks since it is also applied for the communication between such blocks. As previously mentioned, the ability to perform computations within multiple blocks allows the code to address complex geometric configurations.

### Magnetic Diffusion with Ohmic Heating

The exact closed-form analytic solution to the resistive diffusion of magnetic field at constant magnetic diffusivity can be easily implemented to provide the means for verification and sensitivity analysis of the related numerical schemes. In the absence of fluid flow and all other dissipative effects an analytic solution to the energy equation can also be obtained under the ideal gas assumption. In this manner, the Joule heating routines of MHD codes can also be verified along with the ideal equation of state for constant, but finite degree of ionization. Under these assumptions the two relevant equations are:

$$\text{Magnetic Induction:} \quad \frac{\partial \vec{B}}{\partial t} = -\bar{\eta} \vec{\nabla} \times \vec{\nabla} \times \vec{B} = \bar{\eta} [\vec{\nabla}^2 \vec{B} - \vec{\nabla}(\vec{\nabla} \cdot \vec{B})] \quad (3)$$

$$\text{Energy:} \quad \rho \frac{\partial e}{\partial t} = \frac{\bar{\eta}}{\mu_0} (\vec{\nabla} \times \vec{B})^2 \quad (4)$$

where  $\rho$  is constant as a consequence of mass conservation. The one-dimensional, time-dependent solutions to these equations for the magnetic field and temperature can be obtained for all three components of the magnetic field within semi-infinite rectangular or cylindrical coordinates, thus they can also be used for verification of recently emerging 3-dimensional MHD computer codes. In other words, the magnetic field is of the form

$$\vec{B} = B_i(j \perp i, t) \hat{i} \quad ; i, j = x, y, z \text{ or } i, j = r, \theta, z \quad (5)$$

where  $j$  represents the direction of field diffusion. It is noted that equation (3) has not yet invoked Maxwell's condition for a divergence-free field,  $\vec{\nabla} \cdot \vec{B} = 0$ , as it is superfluous to the set of the single-fluid MHD equations. For this 1-dimensional test problem the condition is self-consistently satisfied for 3-D rectangular and 2-D axisymmetric cylindrical geometries that impose only the azimuthal component of the magnetic field. However, using the test problem to verify diffusion of in-plane magnetic fields in cylindrical coordinates, care needs to be taken in appropriately setting up the computational domain or artificially zeroing the extraneous field component.

We can now proceed to impose the  $\vec{\nabla} \cdot \vec{B} = 0$  condition along with the caloric equation of state for an ionized ideal gas,

$$e = (1 + \zeta)C_v T = \frac{(1 + \zeta)RT}{\gamma - 1} \quad (6)$$

to reduce the equations using  $j=z$  as the diffusion direction. Furthermore, it is useful to produce the non-dimensional forms according to the following dimensionless variables:

$$\tau = \frac{t}{t_0}, \quad \xi = \frac{z}{z_0}, \quad b(\xi, \tau) = \frac{B_i(\xi, \tau)}{B_c}, \quad \Theta(\xi, \tau) = \frac{T(\xi, \tau)}{T_0}, \quad \alpha = \frac{\bar{\eta}t_0}{z_0^2}.$$

Substitution of the above relationships reduces equations (3) and (4) to the following one-dimensional form:

$$\frac{\partial b}{\partial \tau} = \alpha \frac{\partial^2 b}{\partial \xi^2} \quad (3A), \quad \frac{\partial \Theta}{\partial \tau} = \frac{\gamma(\gamma - 1)A^2}{a^2} \alpha \left( \frac{\partial b}{\partial \xi} \right)^2 \quad (4A)$$

The analytic solutions for the magnetic field and temperature can be easily produced for a semi-infinite 1-dimensional domain subject to the following boundary and initial conditions:

$$b(0, \tau) = 1, \quad b(\xi, 0) = 0, \quad \text{and} \quad \Theta(\xi, 0) = 1 \quad (7)$$

The solution to the reduced magnetic induction equation is none other than the one-dimensional unsteady diffusion which results in the familiar complementary error function. It can then be integrated to produce the temperature solution via equation (4A). They are as follows:

$$b(\xi, \tau) = \text{erfc}\left(\frac{\xi}{2\sqrt{\alpha\tau}}\right) \quad (8)$$

$$\Theta(\xi, \tau) = 1 + \frac{\gamma(\gamma - 1)V_A^2}{\pi a^2} \int_0^\tau \frac{\exp\left(\frac{-\xi^2}{2\alpha x}\right)}{x} dx = 1 + \frac{\gamma(\gamma - 1)V_A^2}{\pi a^2} \left\{ \text{Ei}\left(\frac{\xi^2}{2\alpha\tau}\right) - \lim_{x \rightarrow 0^+} \text{Ei}\left(\frac{\xi^2}{2\alpha x}\right) \right\} \quad (9)$$

where  $\text{Ei}^*$  represents the Cauchy principal value exponential integral. It is important to note here that the integral involved in the energy equation diverges as  $\xi \rightarrow 0$ . This is a consequence of the imposed magnetic field boundary and initial conditions that introduce infinite currents at the constant-field boundary. This is a common occurrence in modeling real devices since magnetic fields are usually introduced through current-carrying coils. Consequently, inclusion of Ohmic heating through the energy equation allows code users to extend the accuracy and robustness since otherwise acceptable discrepancies will be amplified via the diverging nature of temperature profile.

### **Application**

The MHD code MACH is utilized to provide bilateral confirmation of the test problem. The computational domain is depicted in Figure 1 along with boundary and initial conditions. The numerical setup should be designed to explore the accuracy (and stability whenever applicable) of the diffusion scheme, so once the characteristic dimension  $z_0$  is chosen, the magnetic diffusivity should be varied and the code should be executed for simulation times of the order of the diffusion depth,  $t_0 = z_0^2 / \bar{\eta}$ . To ensure semi-infinite computations the downstream zero-gradient boundary should be extended at least five times the characteristic dimension,  $z_0$ . Conforming execution times to the magnetic field's characteristic diffusion time also assures full capture of the temperature profiles since its characteristic diffusion time will be reduced by the square of the factor,  $f_0 = a^2 / \gamma(\gamma - 1)V_A^2$ . This factor is of course a function of the initial conditions but for most practical applications  $f_0 \ll 1$  and should be designed as so for the verification cases. The prime motivation in defining the initial conditions however, is their effect in enhancing temperature gradients and thus allowing the user to interrogate a code's limitations.

---

\* The Cauchy principal value exponential integral is defined as  $\text{Ei}(y) = \int_{-\infty}^y \frac{e^v}{v} dv$ . Substitution  $v = \frac{-\xi^2}{2\alpha x}$  and subsequent algebraic manipulation leads to the expression appearing in equation (7).

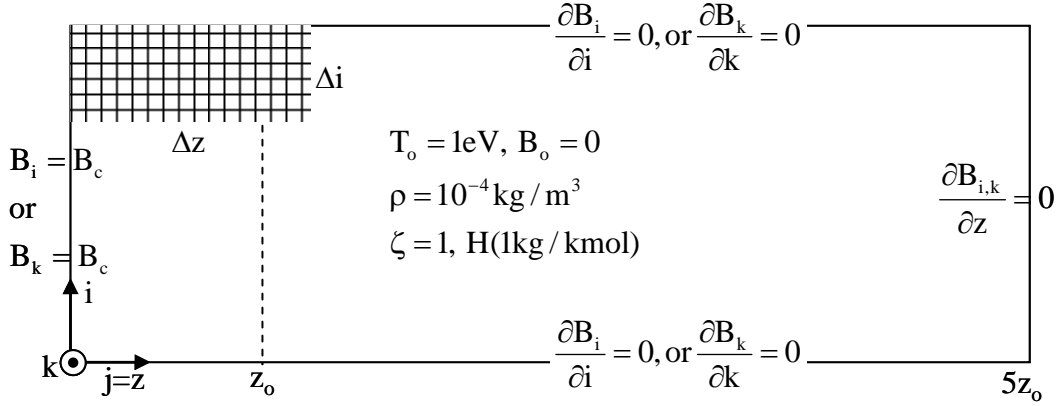


**Figure 1.** Computational set up for the magnetic diffusion with Ohmic heating test case including boundary and initial conditions. The set up is applicable to both rectangular ( $i, k = x, y$ ) and cylindrical coordinates ( $i, k = r, \theta$ ).

The value of inclusion of the energy equation with Ohmic heating to the test problem is that its solution (Equation (9)) diverges as  $\xi \rightarrow 0$  which will in turn significantly test the capabilities and accuracy of a MHD code. Further elaboration of the significance of equation (9) in testing the robustness of a code follows, however it should be noted that the temperature gradient which asymptotes to infinity as  $\xi \rightarrow 0$  is enhanced by a factor  $1/f_0$ . The boundary conditions for the magnetic field should ensure one-dimensionality (see Figure 1) within a semi-infinite region, thus the boundary at the end of the computational domain should employ a zero-gradient boundary condition with respect to the diffusion dimension, i.e.  $z$  for the chosen example depicted by Figure 1. Furthermore, the test case should not employ any temperature boundary conditions, thus codes which do not allow for such option (i.e. codes that have to employ a different set of differential equations at boundaries) are inadequate for the test problem. The MACH code uses a ghost cell technique which extends the computational domain by one additional cell in all directions thus applying the boundary condition to these additional cells and circumventing the need for a different set of equations. In this manner a temperature boundary condition does not have to be defined.

The choice of grid resolution depends on the numerical scheme utilized for the magnetic diffusion equation and is related to the stability/accuracy factor  $\phi = \frac{\bar{\eta} \Delta t}{\Delta j^2}$ . Simple explicit differencing methods are unstable for  $\phi > 1/2$  and they are further limited by accuracy issues as the truncation error is  $\mathcal{O}[\Delta t, \Delta j^2]$ . Accuracy can be substantially enhanced for such schemes if  $\phi = 1/6$  as it improves truncation error to  $\mathcal{O}[\Delta t^2, \Delta j^4]$  but introduces elevated computational time penalties. Implicit schemes are unconditionally stable but are also limited by accuracy issues. MACH employs a simple implicit scheme with successive over-relaxation (SOR) which also introduces truncation error of  $\mathcal{O}[\Delta t, \Delta j^2]$ . Tolerable accuracy is achieved if  $\phi \leq 1/3$ . The associated computational time penalties are mitigated by the introduction of a multi-grid technique that reduces convergence times by utilizing successively coarser grid resolution during iteration. The code was executed for three representative simulations of varying magnetic diffusivity with a grid spacing of  $\Delta j = \Delta z = 3.9\text{mm}$  designed to produce the same profiles. Grid spacing in directions perpendicular to the diffusion direction can be quite coarse as the problem is designed as one-dimensional; the computations shown utilized  $\Delta i = 15.6\text{mm}$ . The magnetic diffusivity was varied by two orders of magnitude thus encompassing a diverse range of plasmas ranging from laboratory plasmas ( $\sim 100\text{m}^2/\text{s}$ ) to space plasmas ( $\sim 10,000\text{m}^2/\text{s}$ ). The computations were performed with constant time-steps,  $\Delta t$ , adhering to  $\phi \leq 1/3$  and the results are shown in Figure 2. The code computes identical magnetic field profiles for all three cases with maximum error less than 1%.

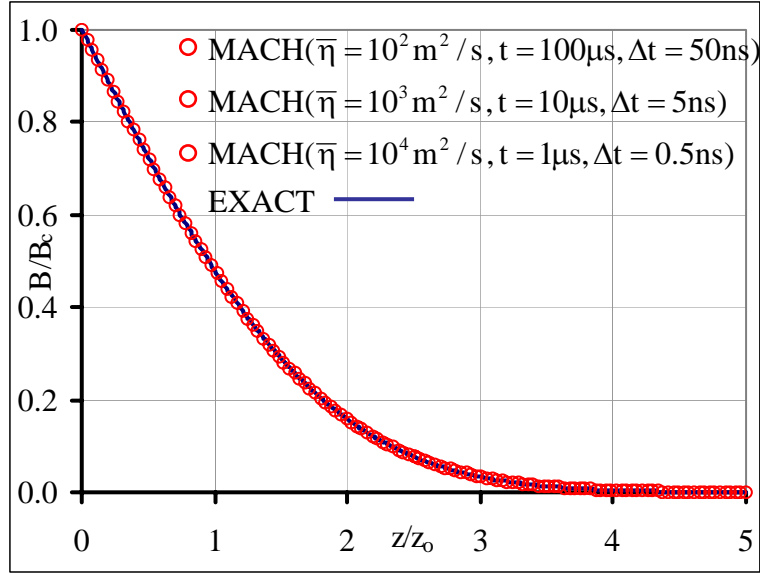


**Figure 2.** Comparisons of computed magnetic field profiles using the MHD code MACH to the exact solution for varying magnetic diffusivity values. ( $z_0=0.1m$ )

Computations of the temperature profiles utilized fully-ionized hydrogen gas at an initial temperature of 1eV, initial density of  $10^{-4} \text{ kg/m}^3$  as depicted by Figure 1 and boundary magnetic field,  $B_c=1T$ . These values correspond to an Alfvén speed,  $V_A=89.21\text{km/s}$ , sound speed,  $a=17.93\text{km/s}$  thus resulting in  $f_0 = 0.036$ . Based on these values the exact solution at  $z=\Delta z$  is 58.7 eV thus the temperature diffusion depth defined as half of this value occurs at approximately  $z = f_0^2 z_0$ . The important aspect of computing the temperature profile is that the relative error introduced by the magnetic field calculation doubles in magnitude and is relatively independent of the conditions. This, in conjunction to the diverging nature of the temperature ( $\xi = z/z_0 \rightarrow 0$ ), serves as an excellent example in illustrating the necessity for elevated accuracy. For example and for the given conditions, numerical error of the order of 10% in the calculation of the magnetic field will result in temperature value errors of the order of 20% which in turn implies that the temperature at  $z=\Delta z$  will be overestimated by about 12eV which is approximately the first ionization potential for hydrogen, (13.6eV). Furthermore, the sensitivity of the solution to relatively small perturbation as  $\xi = z/z_0 \rightarrow 0$  can really test the stability and robustness of the numerical schemes. Such issues will not arise by simply verifying based on just including magnetic field diffusion. The MACH computations show excellent agreement with the exact solution, (see Figure 3) wherein the maximum error naturally occurs a  $z=\Delta z$  and it is less than 1.5%. (It should be noted in Figure 3, as was the case for the magnetic field computations depicted by Figure 2, that the code was executed for all cases shown and produced the exact same results per design. This is the reason for identical symbols utilized by the graphs of Figures 2 and 3 to represent the numerical results.)

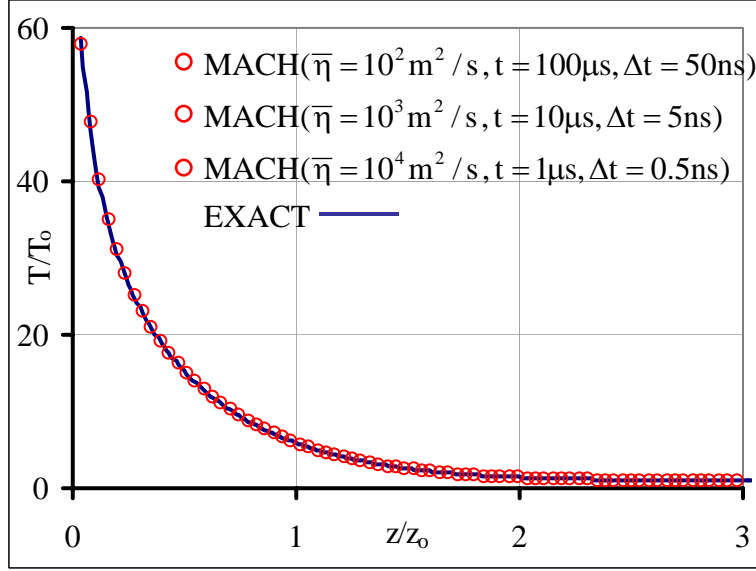


**Figure 3.** Comparisons of computed temperature profiles using the MHD code MACH to the exact solution for varying magnetic diffusivity values. ( $z_0=0.1m$ )

Overall the magnetic diffusion test problem that includes the effects of Joule heating represents a case that can be easily implemented, offers a simple analytic solution but at the same time presents a challenging computational problem in terms of interrogating the robustness and accuracy of a magnetohydrodynamic code.

### Magnetohydrodynamic Shock Tube

The infinite shock tube problem<sup>1</sup> represents a classic test problem for both hydrodynamic (HD) and magnetohydrodynamic (MHD) codes as it allows interrogation of a code's capability in capturing wave propagation including discontinuities arising from contact surfaces and shock waves. It has been extensively used to examine the diffusive or dispersive nature of different numerical schemes<sup>2,3</sup> applicable to nonlinear hyperbolic partial differential equations that prescribe the process of unsteady convection. For the one-dimensional case usually invoked and in the absence of dissipative phenomena the problem is represented by the general conservation law,

$$\frac{\partial U}{\partial t} + \frac{\partial F(U)}{\partial z} = 0 \quad (10)$$

where  $F(U)$  represents the flux vector of the property  $U$  vector. The problem is set up by initially introducing two compartments containing two fluids of different properties; the high-pressure driver gas (region 4 in Figure 4) and the driven gas (region 1 in Figure 4). Upon bursting the diaphragm that separates the two regions a compression wave traveling to the right will coalesce into a shock wave while a fast expansion wave propagates toward the upstream boundary. Dependent on initial conditions different contact discontinuities can be introduced defined by changes in the gas properties while pressure (for the HD shock tube) or full pressure (for the MHD shock tube) and velocity remain continuous.

In the absence of magnetic fields (HD shock tube) an exact closed-form analytic solution to the nonlinear system represented by equation (10) can be obtained, but it is implicit. For the MHD shock tube problem that contains both perpendicular components of the magnetic field to the flow direction no analytic solution has yet been established. For the special case of  $\gamma=2$  (as it will be shown later) for both driver and driven gases an analytic solution can be extracted, however it involves an iterative solution of a set of nonlinear algebraic equations. If the MHD shock problem is introduced involving only one perpendicular component of the magnetic field to the flow direction,  $j=z$ , as follows,

$$\vec{B} = B(z,t)\hat{i} \quad \text{and} \quad \vec{u} = u(z,t)\hat{j} \quad ; i = x, y \text{ or } i = r, \theta \quad (11)$$

then the conservation laws represented by equation (8) expand to the following set:

$$\text{Continuity : } \frac{\partial \rho}{\partial t} + \frac{\partial}{\partial z}(\rho u) = 0 \quad (12)$$

$$\text{Momentum : } \frac{\partial}{\partial t}(\rho u) + \frac{\partial}{\partial z}(P + \rho u^2) = 0 \quad (13)$$

$$\text{Energy : } \frac{Ds}{Dt} = 0 \quad (14)$$

$$\text{Magnetic Induction : } \frac{D}{Dt} \left( \frac{B}{\rho} \right) = 0 \quad (15)$$

Equations 12-14 are none other than Euler's equations for the magneto-fluid where the thermal pressure,  $p$  is replaced by the full pressure,  $P = p + \frac{B^2}{2\mu_0}$  and are sufficient in solving for  $P(z,t)$ ,  $\rho(z,t)$  and  $u(z,t)$  for the whole flow

once the isentropic condition is identified, except of course across the shock wave and contact discontinuities where  $Ds/Dt > 0$ . In the absence of magnetic fields (HD shock tube) the isentropic condition is  $p / \rho^\gamma = \text{constant}$ . The jump conditions across the shock and contact discontinuities can then be obtained through the steady-state formulation of the same conservation laws utilizing the Hugoniot relation for energy conservation. Equation (15) is a consequence of Faraday's Law, Ohm's Law for ideal MHD and continuity, and shows that the quantity  $B/\rho$  is conserved for any fluid element as it convects. Furthermore, equation (15) implies that the magnetic pressure,  $p_m = B^2 / 2\mu_0 = c\rho^2$  where  $c$  is a constant, thus the effective specific heat ratio defined by  $p_m / \rho^\gamma = \text{constant}$  is  $\gamma=2$ . The magnetic pressure behaves like a  $\gamma=2$  gas, so if the fluid is modeled as  $\gamma=2$  gas as well, then the isentropic condition for the MHD shock tube becomes  $P / \rho^\gamma = \text{constant}$  and the energy equation can be written as follows:

$$\text{Energy : } \frac{D}{Dt} \left( \frac{P}{\rho^\gamma} \right) = 0 \quad (16)$$

In this manner the governing equations for the hydrodynamic and magnetohydrodynamic shock tube problems are indistinguishable and thus adhere to the same analytic solution. The well-established solution for the HD shock tube can be applied to the MHD shock tube problem for obtaining  $P(z,t)$ ,  $\rho(z,t)$  and  $u(z,t)$ . Then the magnetic induction equation can be utilized to obtain a solution for  $B(z,t)$  and  $p(z,t)$  and the ideal equation of state for a constant-ionization,  $\zeta$ , gas,

$$p = (1 + \zeta)\rho RT \quad (17)$$

to obtain the temperature,  $T(z,t)$ . It can be easily demonstrated from the energy equation that the speed of wave propagation or effective speed of sound for the  $\gamma=2$  magneto-fluid is  $A = \sqrt{\gamma P / \rho}$ .

The objective of this paper is not to reproduce the process of obtaining an analytic solution to the conservation laws (equations 12-13-15-16) which can be found in a number of good textbooks.<sup>15</sup> Rather, we aim to produce and present a simple analytic solution that can be easily implemented to test the convection numerical schemes of both hydrodynamic and magnetohydrodynamic codes. Moreover, we seek an explicit analytic solution to this classic problem which has never been accomplished before, in doing so a brief description of one method to solve the aforementioned nonlinear system is required.

The continuity, momentum and the isentropic relationships can be utilized to produce the Riemann invariants along characteristics which in turn lead to expressions for all gas properties within the expansion wave. The same conservation laws can then be applied to connect the jump conditions across the moving normal shock using the Hugoniot form of the energy equation. The relationships for the two waves can produce the full solution by applying continuity conditions for the pressure and velocity across otherwise possible contact discontinuities. The method produces the following relationship for the initial pressure ratio,  $P_4/P_1$  and the pressure ratio behind the moving shock wave,  $P_2/P_1$ :

$$\frac{P_4}{P_1} = \frac{P_2}{P_1} \left[ 1 - \frac{(\gamma-1) \frac{A_1}{A_4} \left( \frac{P_2}{P_1} - 1 \right)}{\sqrt{2\gamma \left\{ (\gamma-1) + (\gamma+1) \left( \frac{P_2}{P_1} - 1 \right) \right\}}} \right]^{\frac{-2\gamma}{\gamma-1}} \quad (18)$$

where it is assumed that both driver (region 4) and driven gases (region 1) have the same ratio of specific heats. Such assumption is only necessary for application to the MHD shock tube problem for which  $\gamma=2$ . Equation 18 is an implicit relationship which requires iteration for  $P_2/P_1$  once the initial pressure ratio,  $P_4/P_1$  is defined. However, an explicit solution can be formulated as follows:

Let  $X = \frac{P_2}{P_1}$ ,  $\Pi = \frac{P_4}{P_1}$ , and  $\Lambda = \frac{X}{\Pi} = \frac{P_2}{P_4}$ . If the driver and driven gases are modeled at equal densities,  $\rho_4 = \rho_1$

then  $\frac{A_1}{A_4} = \sqrt{\frac{P_1}{P_4}} = \frac{1}{\sqrt{\Pi}}$ . The equal density condition does not restrict the generality of the problem as the initial

pressure ratio can be varied without limitation by initial temperature variations for the HD shock tube and by both temperature and magnetic field variations for the MHD shock tube case. Applying the convenient definitions for the relevant ratios and after some algebraic manipulation equation 18 becomes

$$\left( \frac{X}{\Pi} \right)^{\frac{\gamma-1}{2\gamma}} = 1 - \frac{(\gamma-1) \frac{X-1}{\Pi}}{\sqrt{2\gamma \left[ \frac{\gamma-1}{\Pi} + (\gamma+1) \frac{X-1}{\Pi} \right]}}. \quad (19)$$

We next take the limit of both sides as the initial pressure ratio goes to infinity,  $\Pi = \frac{P_4}{P_1} \rightarrow \infty$  to produce the following polynomial which is only a function of the specific heat ratio:

$$1 - \frac{(\gamma-1)\Lambda}{\sqrt{2\gamma(\gamma+1)\Lambda}} - \Lambda^{\frac{\gamma-1}{2\gamma}} = 0 \quad (20)$$

The real root of the polynomial represents the finite ratio of the pressure behind the shock wave to the chosen driver-gas pressure,  $P_2/P_4$ , which is reached asymptotically as the latter is driven to infinity. The roots can be found in an iteratively fashion for different values of specific heat ratios and are as follows for relevant gases:

$$\gamma = \frac{5}{3} : \Lambda = 0.44562, \quad \gamma = \frac{7}{5} : \Lambda = 0.46089, \quad \gamma = 2 : \Lambda = 0.43134 \quad (21)$$

Considering the asymptotic nature of the solution to equation 19 and the condition that  $P_2/P_1=1$  for  $P_4/P_1=1$  the following explicit relationship is a very good approximation to the exact solution of equation 18:

$$\frac{P_2}{P_1} = \Lambda \left( \frac{P_4}{P_1} + 1 \right) + (1-2\Lambda) \frac{P_4}{P_1} \exp \left( 1 - \frac{P_4}{P_1} \right) \quad (22)$$

The explicit solution represented by equation 22 is compared to the solution of equation 18 obtained iteratively in Figure 4 for  $\gamma=2$ . Similarly accurate solutions are obtained for any specific heat ratio value and thus can be used for HD shock tube problems using different gases. Furthermore, the process of solving for the root of equation 20 can be extended to HD shock tubes that utilize different  $\gamma$  gases for the driver and driven gases. This is usually desirable in practice since the incident shock strength is increased when low molecular-mass gases are used as the driver gases while high molecular-mass gases are used as the driven gas.

Explicit solutions to all gas properties can now be generated for both HD and  $\gamma=2$  MHD shock tube cases. Considering the conservation laws in the frame of reference of the moving shock wave produces an expression for the speed of the shock wave,  $V_s$ :

$$V_s = A_1 \sqrt{1 + \frac{\gamma+1}{2\gamma} \left[ \Lambda \left( \frac{P_4}{P_1} + 1 \right) + (1-2\Lambda) \frac{P_4}{P_1} \exp \left( 1 - \frac{P_4}{P_1} \right) - 1 \right]} \quad (23)$$

It is useful to reiterate that since  $A = \sqrt{\gamma P / \rho}$ , then for the HD shock tube case this is simply the speed of sound since  $P$  reduces to the thermal pressure,  $p$ . For the  $\gamma=2$  MHD shock tube the full pressure is to be implemented for calculation of the effective speed of wave propagation. The shock speed behind the shock,  $u_2$  is given by

$$u_2 = \frac{A_1}{\gamma} \left[ \Lambda \left( \frac{P_4}{P_1} + 1 \right) + (1 - 2\Lambda) \frac{P_4}{P_1} \exp \left( 1 - \frac{P_4}{P_1} \right) - 1 \right] \sqrt{\frac{2\gamma}{(\gamma + 1) \left[ \Lambda \left( \frac{P_4}{P_1} + 1 \right) + (1 - 2\Lambda) \frac{P_4}{P_1} \exp \left( 1 - \frac{P_4}{P_1} \right) \right] + \gamma - 1}} \quad (24)$$

If the location of the diaphragm is  $z_0$  and since the speed is continuous across contact discontinuities,  $u_2 = u_3$ , the full speed profile can be derived as follows:

$$u(z, t) = \begin{cases} \frac{2}{\gamma + 1} \left( A_4 + \frac{z - z_0}{t} \right) & \text{if } -A_4 \leq \frac{z - z_0}{t} \leq u_2 - A_3 \\ u_2 & \text{if } u_2 - A_3 \leq \frac{z - z_0}{t} \leq V_s \\ 0 & \text{otherwise} \end{cases} \quad (25)$$

where  $A_3 = \left( 1 - \frac{\gamma - 1}{2} \frac{u_2}{A_4} \right) A_4$  is the speed of propagation through the expansion wave derived directly from the

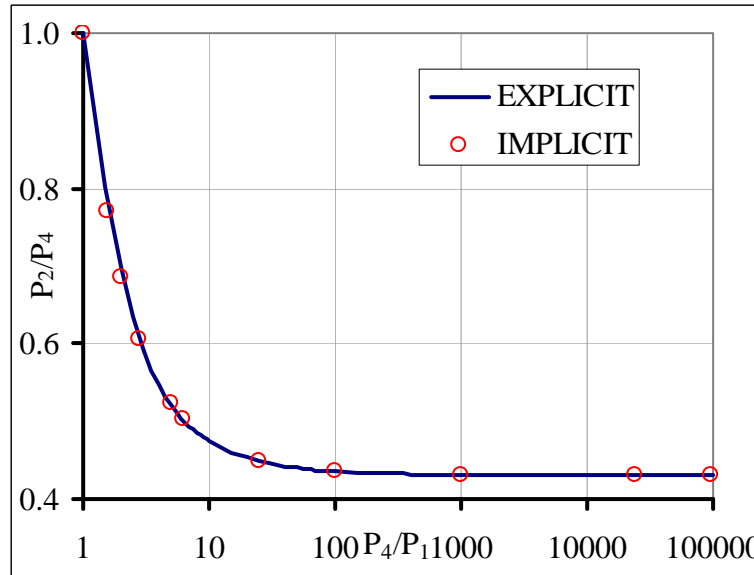


**Figure 4.** Comparisons of the pressure ratio behind the shock ( $P_2/P_4$ ) obtained explicitly through equation 20 to the implicit solution obtained iteratively from equation 18.

Riemann invariants. The pressure is also preserved across contact discontinuities,  $P_3 = P_2$ , which leads to the pressure profile by utilizing the isentropic relationship given as a ratio to the driven gas initial pressure,  $P_1$ :

$$\frac{P(z,t)}{P_4} = \begin{cases} 1 & \text{if } \frac{z-z_0}{t} \leq -A_4 \\ \frac{P_4}{P_1} \left(1 - \frac{\gamma-1}{2} \frac{u(z,t)}{A_4}\right)^{\frac{2\gamma}{\gamma-1}} & \text{if } -A_4 \leq \frac{z-z_0}{t} \leq u_2 - A_3 \\ \Lambda \left(\frac{P_4}{P_1} + 1\right) + (1-2\Lambda) \frac{P_4}{P_1} \exp\left(1 - \frac{P_4}{P_1}\right) & \text{if } u_2 - A_3 \leq \frac{z-z_0}{t} \leq V_s \\ \frac{P_1}{P_4} & \text{if } \frac{z-z_0}{t} \geq V_s \end{cases} \quad (26)$$

Once again we note that the full pressure,  $P$  reduces to the thermal pressure,  $p$  for hydrodynamics and the generated profiles are applicable to any  $\gamma$  gas. For monatomic and diatomic gases the values for  $\Lambda$  are given by equation (21).

Generating the one-dimensional, time-dependent profiles for the remaining variables requires the solution to the conservation laws across contact discontinuities. Specifically, the conservation laws permit a degenerate solution when mass flux is identically equal to zero, ( $\frac{\partial u}{\partial z} = 0 \Rightarrow \frac{\partial P}{\partial z} = 0$ ). The approach<sup>16</sup> is similar to that of shock wave discontinuities previously discussed which establishes the characteristic speed of the contact discontinuity as  $A_4 - \frac{\gamma-1}{8}u_2$ . These contact discontinuities produce density, magnetic-field and temperature gradients that are included in the profiles and are as follows:

$$\frac{\rho(z,t)}{\rho_4} = \begin{cases} 1 & \text{if } \frac{z-z_0}{t} \leq -A_4 \\ \left(1 - \frac{\gamma-1}{2} \frac{u(z,t)}{A_4}\right)^{\frac{2}{\gamma-1}} & \text{if } -A_4 \leq \frac{z-z_0}{t} \leq A_4 - \frac{\gamma-1}{8}u_2 - V_s \\ \frac{V_s}{V_s - u_2} & \text{if } A_4 - \frac{\gamma-1}{8}u_2 - V_s \leq \frac{z-z_0}{t} \leq V_s \\ 1 & \text{if } \frac{z-z_0}{t} \geq V_s \end{cases} \quad (27)$$

where the condition  $\rho_4 = \rho_1$  has been imposed. The magnetic field solution,  $B(z,t)$  can be easily extracted from the magnetic induction, equation (15), which states  $B/\rho = \text{constant}$  and it is presented as a ratio to the driver-gas magnetic field,  $B_4$ . In this manner the solution is applicable to both finite and zero driven-gas magnetic field values,  $B_1$ :

$$\frac{B(z,t)}{B_4} = \begin{cases} \frac{\rho(z,t)}{\rho_1} & \text{if } \frac{z-z_0}{t} \leq A_4 - \frac{\gamma-1}{8}u_2 - V_s \\ \frac{\rho(z,t)}{\rho_1} \frac{B_1}{B_4} & \text{if } A_4 - \frac{\gamma-1}{8}u_2 - V_s \leq \frac{z-z_0}{t} \leq V_s \\ \frac{B_1}{B_4} & \text{if } \frac{z-z_0}{t} \geq V_s \end{cases} \quad (28)$$

The magnetic field profile in conjunction to the full pressure profile given by equation 25 leads to the solution for the thermal pressure,  $p(z,t)$ :

$$p(z,t) = P(z,t) - \frac{B^2(z,t)}{2\mu_0} \quad (29)$$

Lastly, the ideal gas equation of state (equation 17) can be utilized to produce the solution for the temperature profile,  $T(z,t)$ :

$$\frac{T(z,t)}{T_4} = \frac{p(z,t)/p_4}{\rho(z,t)/\rho_4} \quad (30)$$

The set of equations 23-30 constitutes the complete solution to the infinitely-long shock tube problem for a fluid of any uniform specific heat ratio and a magneto-fluid modeled as a  $\gamma=2$  fluid. Furthermore, the set is applicable to cases wherein the magnetic field consists of only one perpendicular component to the flow direction, the initial density values for driver and driven gases are equal, and the flow is modeled at constant (zero or finite) degree of ionization. We now proceed to construct a representative problem that demonstrates the utility of such solution in benchmarking MHD (and CFD) computer codes.

### Application

The details of the computational setup for the magnetohydrodynamic (MHD) shock tube problem are depicted by Figure 5. The case is designed such that contributions from the thermal and magnetic pressures are of equivalent magnitude. In this manner, physical features arising from both pressure and magnetic pressure gradients can be equally tested. Further, the problem can be reduced to a hydrodynamic (HD) shock tube by simply setting the magnetic field values of the driver and driven gases to zero. Then the case can be used for any arbitrary value for the ratio of specific heats. The gas for both driver and driven regions is fully singly ionized hydrogen and the initial density values are equal such that the user can take advantage of the simple explicit analytic solution.

All boundaries have to employ the von Neumann condition for zero-gradient of all variables. In this manner, the

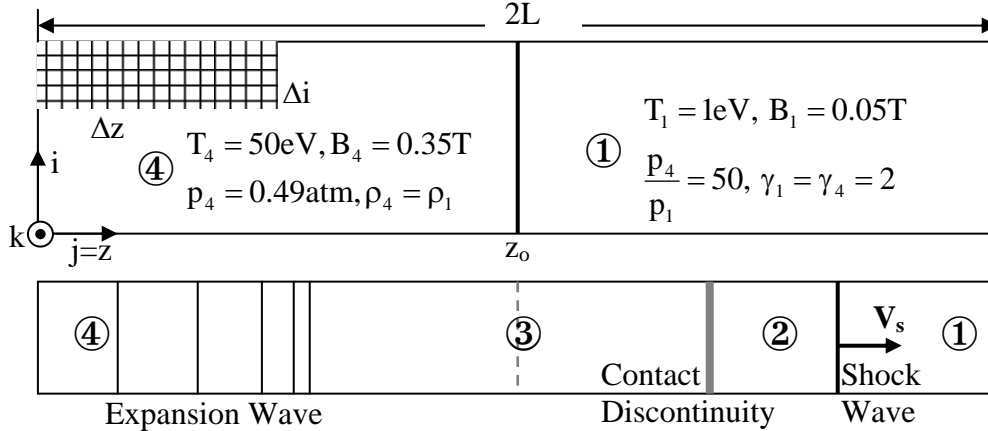


**Figure 5.** Computational set up with initial conditions (top) for the magnetohydrodynamic (MHD) shock tube problem. The gas for both driver (4) and driven (1) regions is fully ionized hydrogen. Bottom schematic shows the relevant physical characteristics at some later time. The setup is applicable to both rectangular ( $i,k=x,y$ ) and cylindrical coordinates ( $i,k=r,\theta$ ).

boundaries defining the region perpendicular to the flow direction ensure one-dimensionality, and the upstream/downstream conditions ensure an infinitely long tube as required. The latter requirement establishes the length of the computational region such that the upstream and downstream conditions do not influence the solution. This can be assured by defining the length of the computational domain sufficiently larger than the fastest transit length which is that of the head of the expansion wave;  $L > A_4 t_f + z_0$  where  $t_f$  is the chosen duration for the computation.

The MHD code MACH is utilized and benchmarked by the analytic solution in figures 6-11. The comparisons are presented for all normalized flowfield properties at  $t_f=3\mu\text{s}$ . Each figure, except the full pressure profile, is augmented by a two-dimensional distribution attached at the bottom to better illustrate the physical structure. The second-order accurate schemes for both flux convection and advancement of the velocity field due to pressure gradients are utilized in these comparisons, so the truncation error is  $\mathcal{O}[\Delta t^2, \Delta z^2]$ . Dispersion has been dampened by application of artificial viscosity. The axial grid resolution is  $\Delta z=2.5\text{mm}$  and the case was executed at a time-step  $\Delta t=10\text{sec}$ . In

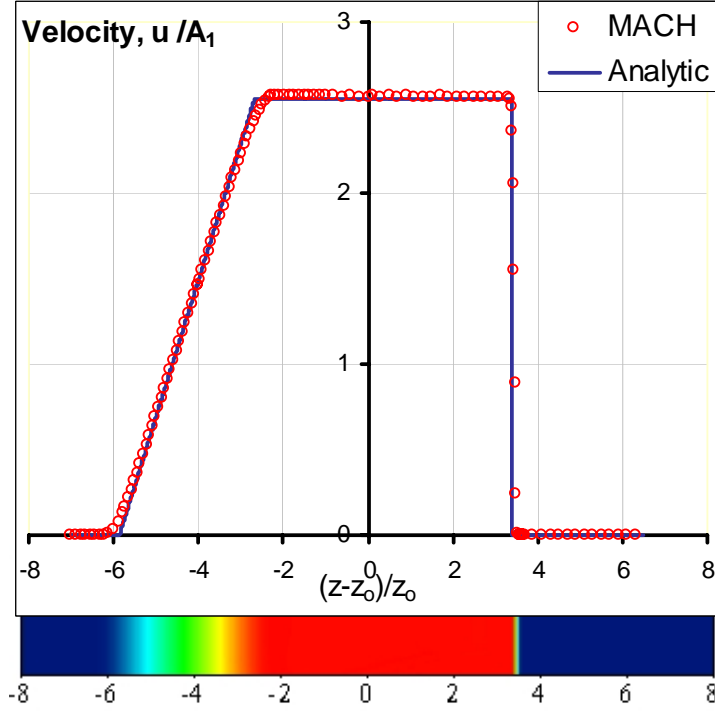


**Figure 6.** Normalized velocity comparisons between MACH and the analytic solution (equation 25) at  $3\mu\text{s}$ . The ordinate crosses the abscissa at the location of the initial diaphragm. ( $z_0=0.1\text{m}$ ,  $A_1=27.783\text{km/s}$ )

this manner the courant condition  $v = \left| \frac{\Delta t}{\Delta z} u_{\text{max}} \right| \leq 1$  is satisfied based on the fastest wave speed which is the propagation of the head of the expansion wave,  $A_4$ . For this representative case  $A_4=195.5\text{km/s}$  which results in  $v=0.78$ . The grid resolution in the direction perpendicular to the flow can be arbitrarily chosen so long as the one-dimensional nature is maintained. For the representative case the one-dimensionality is shown by the two-dimensional contours attached at the bottom of figures 6-10.

The numerical results shown in figures 6-11 do not include every grid point calculation as they have been filtered to avoid clutter. However, all computed points across the shock discontinuity are included to illustrate the degree of shock resolution. The number of points show that the shock wave, which is propagating at  $V_s=113.15\text{km/s}$ , is adequately captured at a thickness of  $\pm 3\Delta z$ . If desirable, improvements can be achieved in resolving the shock thickness by reducing or eliminating artificial viscosity, which was applied for this case, along with reduction of the time-step. However, for second order schemes such as the ones utilized by MACH, this reduction in dissipation can lead to numerical dispersive oscillations. Further, it can lead to oscillations in resolving the contact discontinuity that in turn may not adequately maintain the velocity and full pressure continuity. Such continuity is correctly computed by MACH as illustrated by the velocity (figure 6) and full pressure (figure 11) profiles. The contact discontinuity is located at

$$\left. \frac{z - z_0}{z_0} \right|_{\text{CD}} = \frac{t_f}{z_0} \left( A_4 - \frac{\gamma - 1}{8} u_2 - V_s \right) \quad (29)$$

which is 2.2 for  $t_f=3\mu\text{s}$  duration and the computed profiles show excellent uniformity across the location. The comparisons also show very good agreement in capturing the expansion wave traveling upstream. The dissipation is minimal and the maximum discrepancy does not exceed 2%. The slope of the velocity profile across the expansion wave is  $\frac{\partial u}{\partial z}(t) = \frac{2}{(\gamma + 1)t}$  and can serve for more detailed comparisons. The density, magnetic field, temperature

and thermal pressure comparisons (figures 7-10) also show the same agreement for the shock and expansion waves.

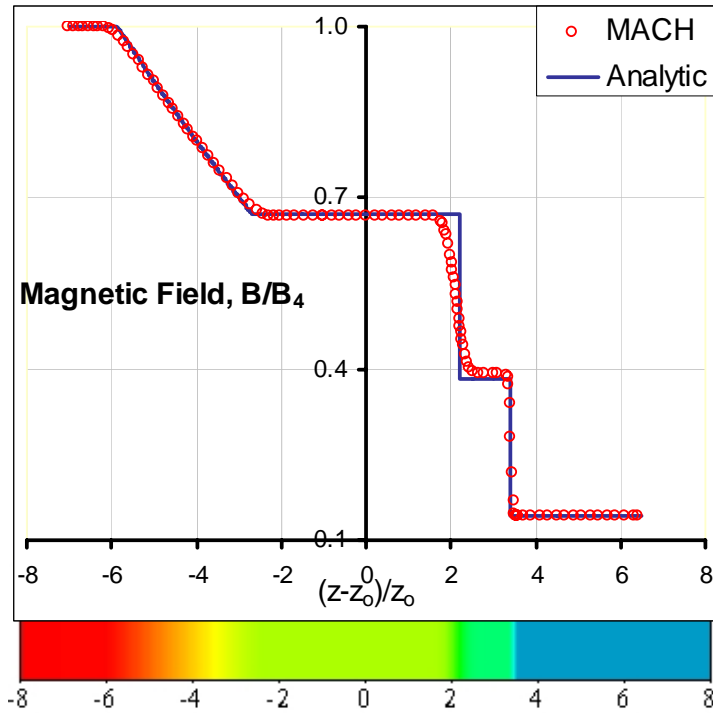


**Figure 7.** Normalized magnetic field comparisons between MACH and the analytic solution (equation 28) at  $3\mu\text{s}$ . The ordinate crosses the abscissa at the location of the initial diaphragm. ( $z_0=0.1\text{m}$ ,  $B_4=0.35\text{T}$ ,  $B_1=0.05\text{T}$ )

However, these also allow comparisons of the quality of the numerical solution regarding resolution of the contact discontinuity. For the specific numerical algorithm used in this case the MACH code shows elevated dissipation in resolving the contact discontinuity as compared to that of the shock wave. This behavior is typical of such second order schemes since the Courant number based on the contact discontinuity's speed of propagation is reduced which leads to higher dissipation. Improvements can be achieved by reducing the time-step and artificial viscosity at the expense of increasing dispersive oscillation. The degree of such trade-off should be evaluated based on each case even though a monotonic behavior is generally desired. Overall, such contact discontinuities will not be maintained in real problems due to diffusive processes such as heat conduction and magnetic diffusion. These real dissipative phenomena will not allow such discontinuities to persist for an appreciable length of time, so it may not be worthwhile to pursue improvements in the quality of the numerical solution.

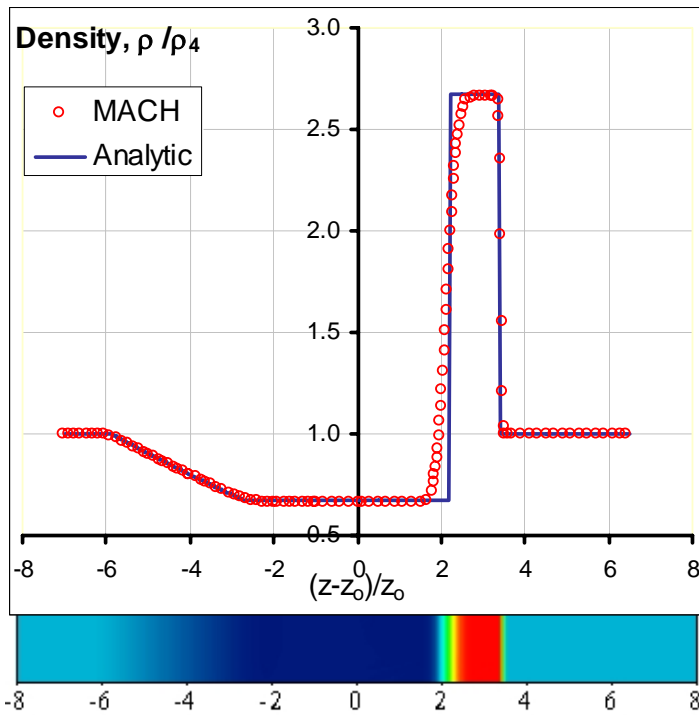


**Figure 8.** Normalized density comparisons between MACH and the analytic solution (equation 27) at  $3\mu\text{s}$ . The ordinate crosses the abscissa at the location of the initial diaphragm. ( $z_0=0.1\text{m}$ ,  $\rho_4=\rho_1=5.1546\times 10^6\text{kg/m}^3$ )

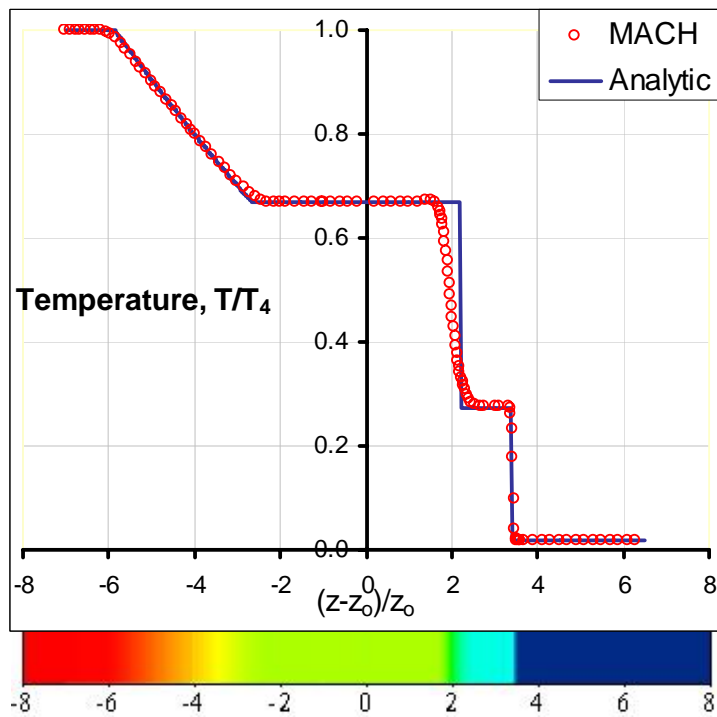


**Figure 9.** Normalized temperature comparisons between MACH and the analytic solution (equation 30) at  $3\mu\text{s}$ . The ordinate crosses the abscissa at the location of the initial diaphragm. ( $z_0=0.1\text{m}$ ,  $T_4=50\text{eV}$ ,  $T_1=1\text{eV}$ )

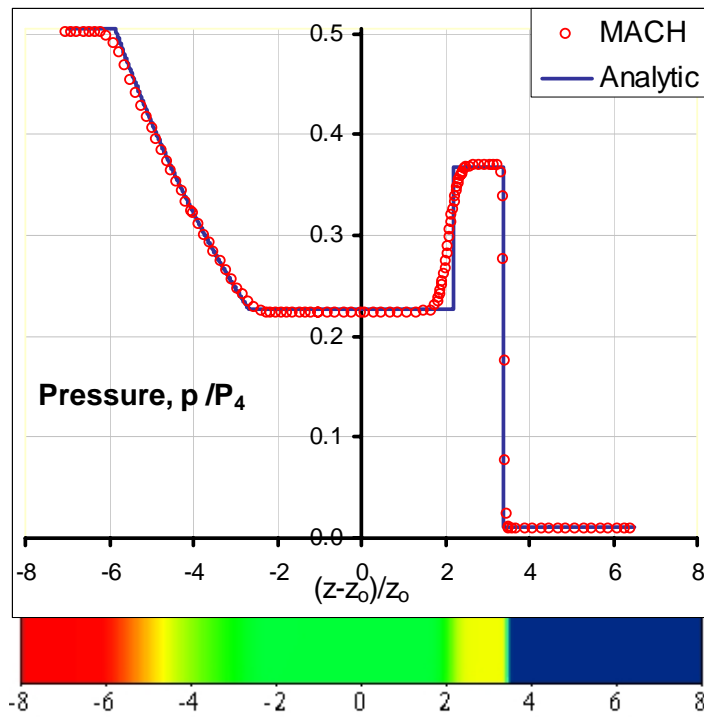


**Figure 10.** Normalized pressure comparisons between MACH and the analytic solution (equation 29) at  $3\mu s$ . The ordinate crosses the abscissa at the location of the initial diaphragm. ( $z_0=0.1m$ ,  $P_4=0.9719atm$ )

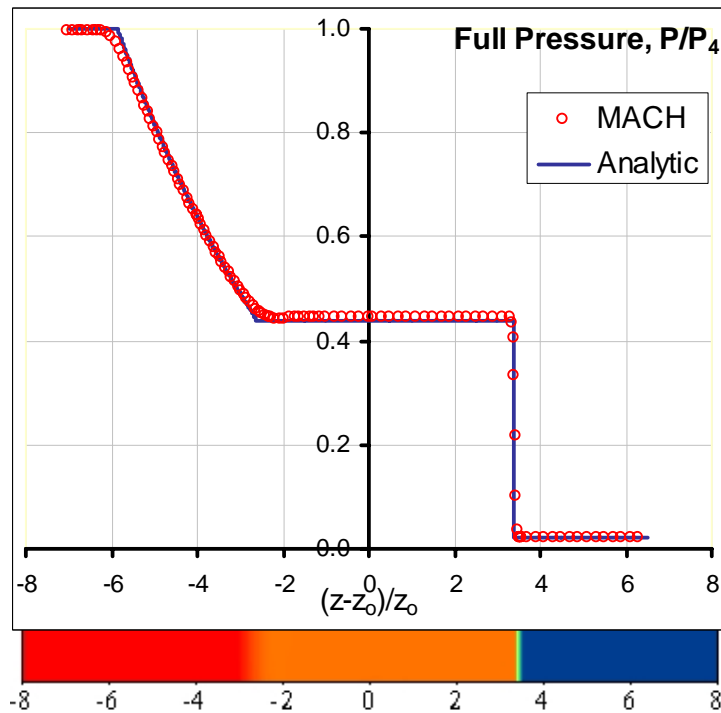


**Figure 11.** Normalized full pressure  $P = p + \frac{B^2}{2\mu_0}$  comparisons between MACH and the analytic solution (equation 26) at  $3\mu s$ . ( $z_0=0.1m$ ,  $P_4=0.9719atm$ )

## Summary

Two idealized plasma physics problems are designed, their closed-form analytic solutions are presented and applied for magnetohydrodynamic (MHD) code verification and benchmarking. The first test case aims to assess magnetic diffusion algorithms and it is combined with joule heating effects that invoke the energy equation. In the absence of any other dissipative effects the solution for the temperature diverges as the constant field boundary is approached. The diverging nature of the solution serves as a challenging check for the accuracy and stability of the pertinent numerical schemes. The second test case presents a unique explicit solution to the Riemann problem for a magnetohydrodynamic shock tube which is an ideal problem to benchmark the numerical solution to nonlinear hyperbolic equations. The case was designed such that both shock and contact discontinuities are present. The solution is outlined in simple, directly applicable formulation for ease of implementation and it is applicable to both hydrodynamic (CFD) and MHD codes. The MHD code MACH was utilized to model both plasma problems and the numerical results were compared to the analytic solutions. This served as bi-lateral confirmation and established a reference for benchmarking the performance of various numerical schemes.

## References

---

- [1] Riemann, B. "Über die Fortpflanzung ebener Luftwellen von endlicher Schwingungsweite," *Abhandlungen der Gesellschaft der Wissenschaften zu Göttingen, Mathematisch-physikalische Klasse* 8, 43, 1860.
- [2] Sod, G.A. "A Survey of Several Finite Difference Methods for Systems of Nonlinear Hyperbolic Conservation Laws," *Journal of Computational Physics*, Vol. 27, 1-31, 1978.
- [3] Brio, M and Wu, C.C. "An Upwind Differencing Scheme for the Equations of Ideal Magnetohydrodynamics," *Journal of Computational Physics*, Vol. 75, 400-422, 1988.
- [4] Peterkin, R.E., Jr., and Frese, M.H., "MACH: A Reference Manual - First Edition," Air Force Research Laboratory: Phillips Research Site, July 10, 1998.
- [5] Frese, M.H., "MACH2: A Two-Dimensional Magnetohydrodynamics Simulation Code for Complex Experimental Configurations," AMRC-R-874, September 1986.
- [6] Peterkin, R.E., Jr., and Frese, M.H., "A Material Strength Capability for MACH2," MRC/ABQ-R-1191, October 1989.
- [7] Mikellides, P.G., "A Theoretical Investigation of Magnetoplasma Thrusters," Ph.D. Dissertation, Department of Aeronautical and Astronautical Engineering, The Ohio State University, 1994.
- [8] Douglas, M.R., "Radiation Production from Stagnating Compact Toroids Employing a Nonequilibrium Radiation Diffusion Model," Ph.D. Dissertation, U. of New Mexico, 1994.
- [9] Braginskii, S.I., "Transport Processes in a Plasma," in *Review of Plasma Physics*, M.A. Leontovich, ed. Consultants Bureau, New York, 1965.
- [10] Degnan, J.H., Peterkin, R.E., Jr. et. al., "Compact Toroid Formation, Compression, and Acceleration," *Physics of Fluids*, B5 (8), 2938, 1993.
- [11] Holian, K.S., ed, "T-4 Handbook of Material Properties Data Base.. Vol Ic: EOS," LA-1160-MS, Los Alamos National Laboratory, Los Alamos, NM, November, 1984.
- [12] Ames, W.F. Numerical Methods for Partial Differential Equations, 2<sup>nd</sup> Ed., Academic, New York, 1977.
- [13] Brandt, A. "Multi-level adaptive solutions to boundary value problems," *Mathematics of Computation*, Vol. 31, No. 138, April 1977.
- [14] van Leer, B. "Towards the Ultimate Conservative Difference Scheme. IV. A New Approach to Numerical Convection," *Journal of Computational Physics*, Vol. 23, 276-299, 1997.
- [15] Anderson, J.D. Modern Compressible Flow With Historical Perspective, Ch. 7, p. 261, 3<sup>rd</sup> Ed. McGraw-Hill, 2003.

---

[16] Courant, R. and Friedrichs, K.O. Supersonic Flow and Shock Waves, Ch. III, p. 126, Pure and Applied Mathematics, Vol I, Interscience Publishers, Inc., New York, 1948.